Bandwidth Expansion of Circular Phased Arrays Through Quasi-Conformal Transformation Optics

Edward Wawrzynek, Songyi Yen, and Dejan Filipovic
University of Colorado Boulder, CO, USA {edward.wawrzynek,songyi.yen,dejan.filipovic}@colorado.edu

***Abstract*—This work proposes a lens design for circular phased arrays using quasi-conformal transformation optics (QCTO) to expand pattern bandwidth. The lenses are designed to partially collimate radiation from array elements, causing the element phase center to move inward with increasing frequency. This phase center motion allows the array to maintain alias-free patterns at higher frequencies. Simulation of the lens structure shows that lens-loading helps maintain directivity and reduced sidelobe levels at higher frequency compared to their unloaded counterparts.**

I. Introduction

Circular arrays find a wide range of applications, including in communications, direction finding, and radar [1], [2]. In particular, circular arrays offer various multifunctional features, including the ability to realize a 360° scan in azimuth, null forming, and combined omnidirectional and directional operation.

Realizing broadband operation of circular arrays is limited by the requirements of element spacing. The upper frequency bound of said arrays' operation is limited by the onset of spatial aliasing in the radiation patterns, which creates insuppressible lobes analogous to the grating lobes observed in linear arrays [3]. This work proposes lens loading for circular arrays to push the onset of this phenomenon to higher frequency.

The proposed lens array is shown in Fig. 1. For the model considered in this work, each element consists of an outward-oriented Huygens source, denoted as a blue dot. Polarization is transverse to the plane. The lenses are designed to partially collimate the radiation from the sources, causing the phase center of the element pattern to move inwards with increasing frequency. This phase center motion allows the array to meet the sampling criterion for alias-free patterns at higher frequencies, thus expanding the pattern bandwidth.

This work uses quasi-conformal transformation optics (QCTO) [4], [5] to design lens loading for circular arrays. The QCTO technique has been used to design collimating lenses for single antenna elements [6], [7], single-element multibeam antennas [8], and lenses with multiple radiating elements embedded within them [9]. However, this work focuses on the effect that such lenses have on the phase relationship between elements in a phased array context.

II. Lens Design

In the QCTO formulation, a desired coordinate transform from a virtual space to a physical space is specified, prescribing a material distribution in the physical space which realizes the effect of the coordinate transform on the electromagnetic

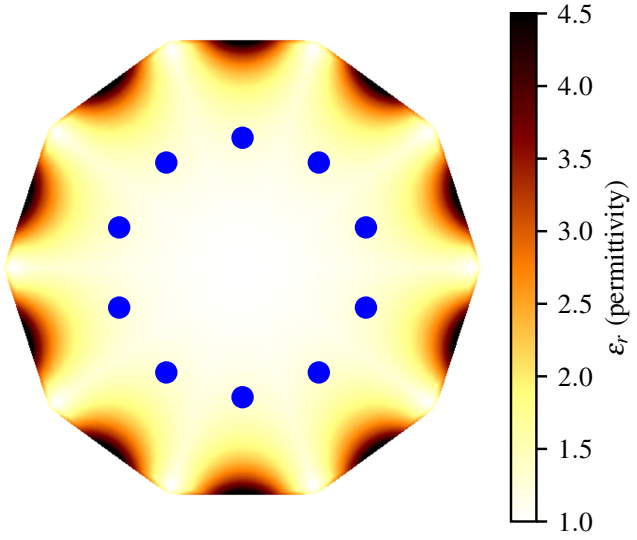

Fig. 1. Permittivity profile for the proposed lens loading of a 10-element circular array. Blue dots mark the locations of the Huygens source elements.

fields. The virtual and physical spaces employed in the lens design are shown in Fig. 2. An upwards radiating Huygens source is embedded in the virtual space. A portion of the upper boundary of the virtual space is formed from a 100° arc centered at that source, which captures a portion of a constant phase front radiating from the source. This arc is transformed into a line in the physical space, collimating a portion of the radiation. This collimation is intended to move the apparent phase center of the source downwards.

A conformal transform between the two spaces is found numerically through the inverse Laplace equation formulation of [10]. The conformal moduli are matched by adjusting the virtual space's height. The lens is designed to be excited by an E-field polarized entirely transverse to the plane, which allows the transform to be realized by a purely isotropic dielectric material, whose distribution is shown in Fig. 3. The permittivity distribution for the lens is taken from a triangular region of the physical space, whose horizontal extent corresponds to the extent of the 100° arc in the virtual space. The full 10-element lens array is formed by arranging these regions in a circle, shown in Fig. 1.

The upper boundary of the virtual space has discontinuities in its derivatives where it transitions from the arc to linear segments on either side. Changing the angle of these segments relative to the arc allows the degree of concentration of the

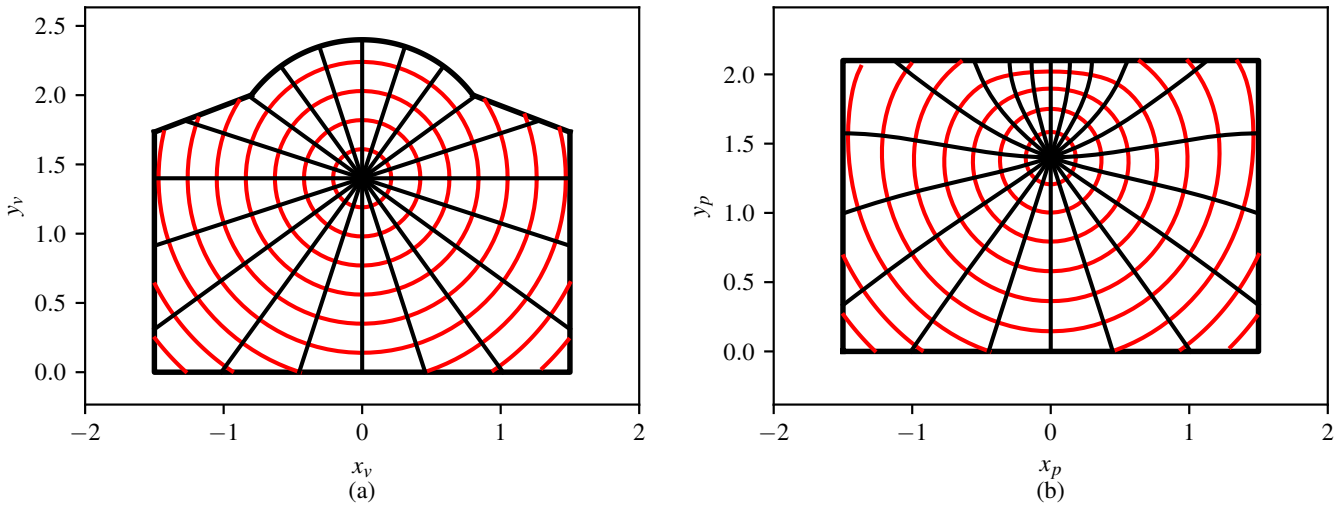

Fig. 2. The layout of (a) the virtual space and its mapping onto (b) the physical space. The red arcs mark curves of constant phase as radiated from the focal point of the virtual space. Black radial lines denote the orientation of the Poynting vector as radiated from this focal point.

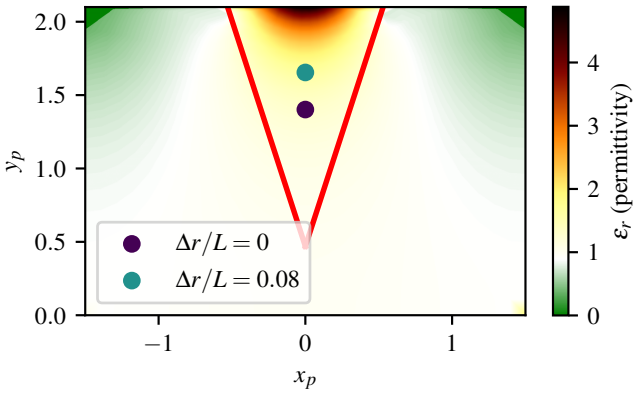

Fig. 3. Permittivity profile of the physical space of Fig. 2(b). The triangular region used to form the lens is marked by the red lines. The purple dot marks the source location which results in uniform phase across the top of the lens; the green dot marks the defocal source location actually used for excitation (see text).

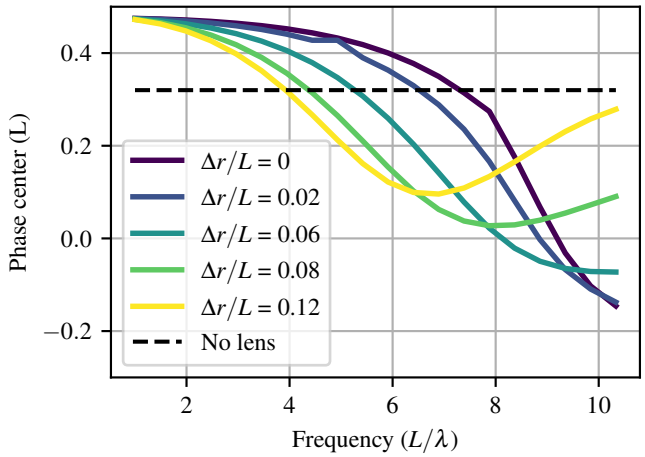

Fig. 4. Radial phase center of the element pattern, with and without lens loading present. The phase center is computed over the central 36° sector of the radiation pattern. Phase center location is plotted in terms of total lens array diameter (L).

high permittivity near the lens edge to be adjusted. The angle of these segments is chosen to maximize the angular extent of the arc which is collimated while avoiding superluminal (i.e., $\epsilon_r < 1$) permittivity in the lens region.

III. Lens Performance

The lens is simulated in two dimensions by numerical solution of the electric field wave equation with an inhomogeneous dielectric. The sources are modeled as point Huygens sources, thus ignoring any mutual coupling between them.

Because the primary purpose of the lens loading is to create phase center motion, defocal excitation of the lens is considered. The radial position of the Huygens source is swept outwards from the focal point of the lens towards its edge by an amount Δr, with the resulting phase center motion shown in Fig. 4. Phase center is calculated as in [11]. The frequency is characterized in terms of the maximum lens array diameter L with respect to wavelength (λ).

At low frequencies, the phase center is close to the outer edge of the array, where the lens aperture is located. This is expected from this aperture's small electrical size—at $L = 1\lambda$, the width of a single lens element is only $l = 0.305\lambda$ across.

With increasing frequency, the collimating effect of the lens drives the phase center inwards. This can be understood by considering the focal point of a single lens aperture. With no defocusing, the aperture is excited with uniform phase, which corresponds to a focal point located infinitely far behind the lens. The finite electrical width of the aperture results in a beam with a phase center located only a finite distance behind the lens, with this distance growing as the electrical size of the aperture increases. Defocal excitation adds curvature to the phase profile excited across the aperture. This corresponds to a focal point located a finite distance behind the lens, with the focal point moving closer to the lens with more defocusing.

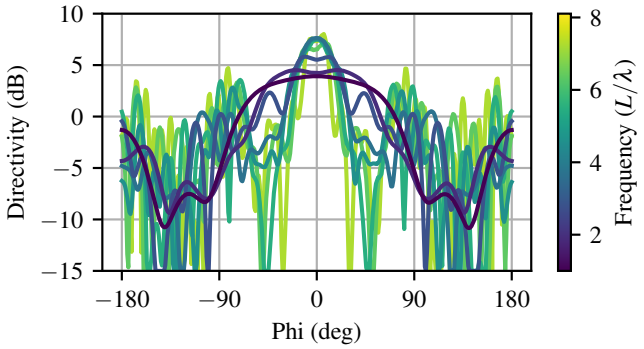

Fig. 5. Radiation pattern of a single element in the lens. Frequency is in terms of lens array diameter (L) with respect to wavelength (λ).

However, more extreme defocusing is observed to increase the initial rate at which the phase center moves backwards, which is desirable for the frequency range considered for array operation. For the array proposed in this work, a defocusing parameter of $\Delta r/L = 0.08$ is selected.

The element patten with lens loading is shown in Fig. 5. As frequency increases, the beamwidth is narrowed by the collimating effect of the lens. Significant sidelobes near $\phi = \pm 80^\circ$ are present above $L = 4\lambda$, caused by spillover as some of the source power illuminates neighboring lenses.

IV. Array Performance

A. Circular Modes

The array is scanned through the use of circular phase modes [1], [2]. In short, the far field pattern $E(\phi)$ is expanded into a Fourier series of circular phase modes with coefficients A_m,

$$E(\phi) = \sum_{m=-\infty}^{\infty} A_m e^{jm\phi}. \tag{1}$$

Because (1) takes the same form as the relationship between port excitation and the far field of a linear array, the circular modes are analogous to port excitation of a linear array. Maximum directivity is achieved with uniform circular mode excitation, scanning is achieved by increasing the phase of successive modes, and tapering can be applied to control sidelobes. However, the relationship between the circular modes and port excitations is more complicated than the linear array.

Let the pattern of a single element $EL(\phi)$ with the lens aperture located at the origin be expanded in a Fourier series

$$EL(\phi) = \sum_{p=-\infty}^{\infty} D_p e^{jp\phi}. \tag{2}$$

Then the amplitude of the m-th circular mode in far field (A_m) and at the array elements (C_m) are related by [1]

$$\frac{A_m}{C_m} = \sum_{p=-\infty}^{\infty} D_p j^{m-p} J_{m-p}\left(\frac{k_0 L}{2}\right), \tag{3}$$

where J_l is the Bessel function of the first kind and k_0 is the wavenumber. Equation (3) gives the port modal excitation, C_m, in terms of the desired far field mode, A_m. Then the voltage to be excited on the n-th port of the array is

$$V_n = \sum_{m=-\infty}^{\infty} C_m e^{j(2\pi nm/N)}, \tag{4}$$

where $N = 10$ is the number of array elements. Only N distinct circular modes can be excited in an N port array, a consequence of the sampling theorem applied to (4).

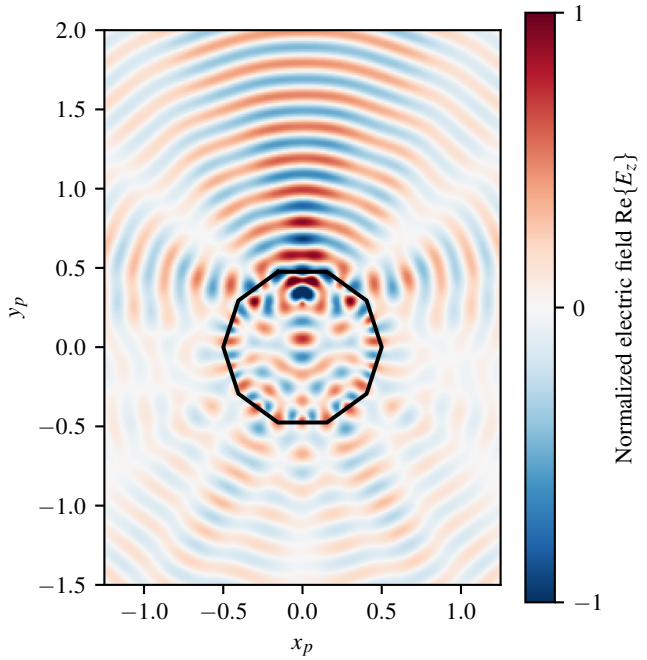

Fig. 6. Near fields of the array at frequency $L = 5\lambda$ when scanned towards $\phi = 90^\circ$. The outline of the lens is shown in black.

B. Array Scanning

The near fields of the array scanned with uniform circular mode excitation at $L = 5\lambda$ are shown in Fig. 6. The elements near the direction of the desired beam are excited most strongly, with excitation of the other elements in the array acting mostly to reduce sidelobes. The collimating effect of the lens can be observed in the flattened phase profile along the top of the lens aperture. Standing waves within the lens and surface waves around the circumference of the lens are apparent, an undesirable effect likely due to the level of mismatch at the lens aperture. This phenomenon may also increase mutual coupling in a practical implementation if not treated.

Scanned patterns of the array are shown in Fig. 7 for two frequencies $L = 1\lambda$ and $L = 5\lambda$. Fig. 7(a) shows patterns for uniform circular mode excitation. At the lower frequency the array performs similarly both with and without the lenses present, suggesting that the elements are spaced tightly enough on their own to realize operation free of spatial aliasing. At the higher frequency, however, the pattern without the lens suffers from a 4 dB drop in directivity and sidelobes within 3

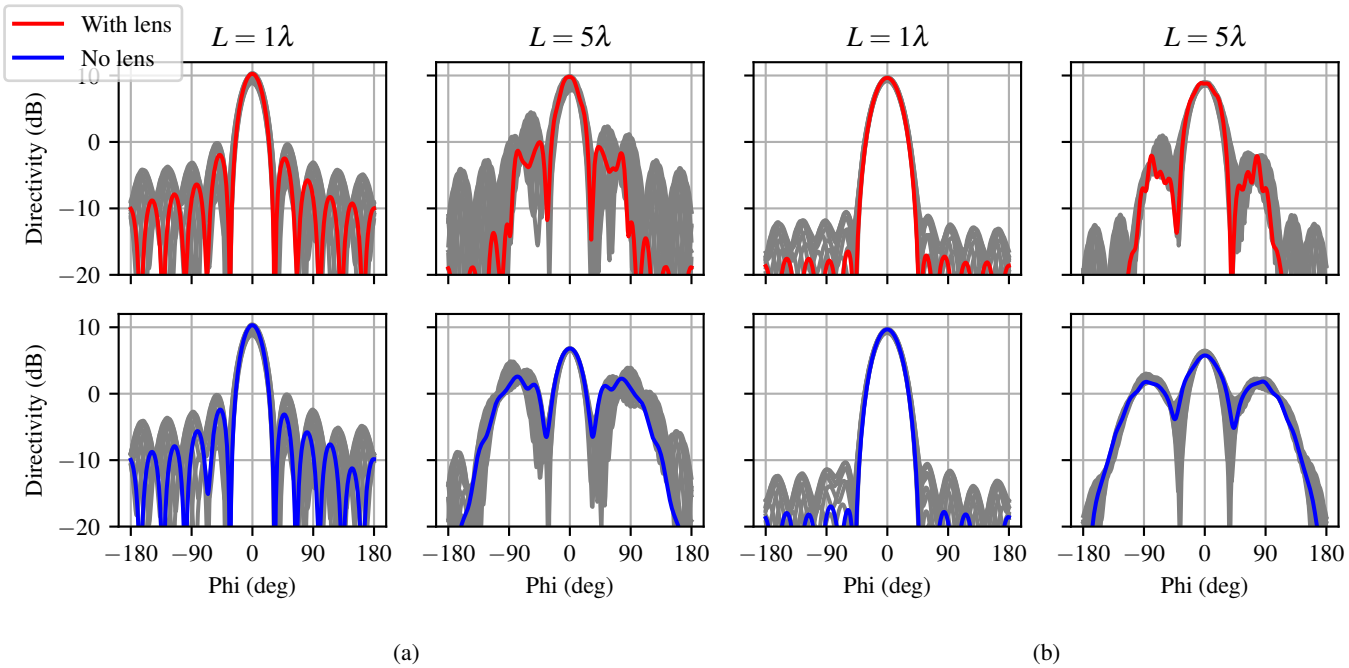

Fig. 7. Scanned patterns of the array with the lens (top row) and without the lens (bottom row). Scanning is shown (a) with uniform excitation of all circular modes and with (b) circular mode excitation weighted by a Taylor window. The red and blue curves are the pattern when scanned in the direction of an element, while the gray curves are the pattern variation as the beam is scanned across the entire 360° range in azimuth. The patterns are shown at two frequencies $L = 1\lambda$ and $L = 5\lambda$.

dB of the mainlobe. The high frequency pattern with the lenses maintains its directivity but does exhibit elevated sidelobes.

Fig. 7(b) shows patterns when the circular modes are weighted by a Taylor window specified for -30 dB sidelobes. At the low frequency, this weighting is effective in reducing the sidelobes for both the array with and without the lenses. At the high frequency, the weighting applied to the array with lenses reduces the peak sidelobe level by 4 dB. When the weighting is applied to the array without lenses it has little effect on the peak sidelobe level nor on the mainlobe directivity. This suggests that the sidelobes in the array without lenses are a consequence of spatial aliasing, which the lens loading partially succeeds in addressing.

V. Conclusion

Lens loading of elements in a circular phased array is demonstrated moving the elements' phase centers inward with increasing frequency. This serves to alleviate undersampling concerns as frequency increases. Simulation of the lens added to an array of Huygens sources shows that it is effective in stabilizing beam directivity and reducing sidelobe levels when compared to the array without the lens. This suggests the possibility that such an approach could broaden the pattern bandwidth of practical circular arrays. Further work is needed to investigate transforms to address lens mismatch and sidelobe formation, as well as broadband antennas for lens excitation and realizations of such arrays. Mutual coupling is not considered in this work but is a critical parameter of study for future works as well.

Acknowledgement

The authors thank Benjamin Cross for helpful discussions. This work was supported by the Office of Naval Research under the grant N00014-24-1-2191.

References

[1] D. E. N. Davies, "Circular arrays," in *The Handbook Antenna Design*, vol. 2. London, U.K.: Peregrinus, 1983, ch. 12.

[2] L. Josefsson and P. Persson, *Conformal Array Antenna Theory and Design*. Piscataway, NJ, USA: IEEE Press, 2006.

[3] M. A. Elmansouri, J. Ha, and D. S. Filipovic, "Ultrawideband TEM horn circular array," *IEEE Trans. Antennas Propag.*, vol. 65, no. 3, pp. 1374–1379, Mar. 2017.

[4] J. B. Pendry, D. Schurig, and D. R. Smith, "Controlling electromagnetic fields," *Science*, vol. 312, pp. 1780–1782, 2006.

[5] J. Li and J. B. Pendry, "Hiding under the carpet: A new strategy for cloaking," *Phys. Rev. Lett.*, vol. 101, pp. 203901/1–4, 2008.

[6] M. Ebrahimpouri and O. Quevedo-Teruel, "Bespoke lenses based on quasi-conformal transformation optics technique," *IEEE Trans. Antennas Propag.*, vol. 65, no. 5, pp. 2256–2264, May 2017.

[7] J. Xu et al., "Multiobjective optimization of bespoke gradient-index lenses: A powerful tool for overcoming the limitations of transformation optics," *Phys. Rev. Appl.*, vol. 18, no. 2, Aug. 2022, Art. no. 024021.

[8] Q. Wu, Z. H. Jiang, O. Quevedo-Teruel, J. P. Turpin, W. Tang, and Y. Hao "Transformation optics inspired multibeam lens antennas for broadband directive radiation," *IEEE Trans. Antennas Propag.*, vol. 61, no. 12, pp. 5910–5922, Dec. 2013.

[9] E. Wawrzynek, S. Yen, and D. Filipovic, "Design of Circular Array Lenses Through the Quasi-Conformal Transformation Optics", *Proc. United States Nat. Committee URSI Nat. Radio Sci. Meeting,*, Boulder, CO, USA, Jan. 2026.

[10] Z. Chang, X. Zhou, J. Hu, and G. Hu, "Design method for quasi-isotropic transformation materials based on inverse Laplace's equation with sliding boundaries," *Opt. Exp.*, vol. 18, pp. 6089–6096, 2010.

[11] P. N. Betjes. "An algorithm for automated phase center determination and its implementation," *Proc. Antenna Meas. Technol. Assoc. Annu. Symp.*, St. Louis, MO, USA, Nov. 2007, pp. 190–195.